ATLAS NOTE

ATLAS-CONF-2011-021

March 11, 2011

A measurement of the ATLAS muon reconstruction and trigger efficiency using J/ψ decays

The ATLAS collaboration

Abstract

We present a measurement of the ATLAS muon reconstruction and trigger efficiencies using decay muons from the J/ψ resonance. The measurement is based on the "tag and probe" method and uses a sample of *p*-*p* collisions at a center-of-mass energy of $\sqrt{s} = 7$ TeV, corresponding to an integrated luminosity of 3.1 pb^{-1}.

To be submitted to *next conference*

1 Introduction

This note describes a measurement of the muon identification efficiency in the first-pass reconstruction of ATLAS data and the trigger efficiency of the ATLAS detector for muons with low transverse momentum, p_{T}. The efficiencies were determined using the so-called “tag and probe” method at the J/ψ resonance. In this method muon pairs are selected by requiring a well reconstructed muon, the “tag”, and an inner detector (ID) track, the “probe”, consistent with coming from a $J/\psi \to \mu^+\mu^-$ decay. In this way the “probes” are selected independently of the ATLAS muon spectrometer (MS) and can be used to measure the efficiency for reconstructing a muon based on the MS. The reconstruction efficiency could be measured with this method up to $p_{\mathrm{T}} = 12$ GeV. With additional requirements on the energy deposit in the calorimeters associated to the probe tracks, the background could be reduced significantly and the measurement could be extended to $p_{\mathrm{T}} = 20$ GeV.

This study was performed with a sample of p-p collisions at $\sqrt{s} = 7$ TeV, collected in the period April-August 2010, corresponding to an integrated luminosity of $3.1\,\mathrm{pb}^{-1}$. The efficiencies presented in this note are currently used in the measurement of the J/ψ production cross section [1] based on the same data sample.

A study of the muon efficiency at larger p_{T}, exploiting the Z resonance is reported in [2]. Early results on the performance of the ATLAS muon system have been presented in [3].

2 The ATLAS Detector

A detailed description of the ATLAS Detector can be found elsewhere [4]. Muons are independently measured in the ID and in the MS.

The ID measures tracks up to a pseudorapidity $|\eta| = 2.5$ exploiting three types of detectors operated in a solenoidal magnetic field of 2 T: a silicon pixel detector closest to the interaction point, a silicon strip detector (SCT) surrounding the pixel detector, and a transition radiation straw tube tracker (TRT) as the outermost part of the inner detector.

The MS consists of large air-core superconducting toroidal magnets, providing a field of approximately 0.5 T. The deflection of the muons in the magnetic field is measured by three layers of precision drift tube (MDT) chambers for $|\eta| < 2.0$ and, for $2.0 < |\eta| < 2.7$, by two layers of MDT chambers in combination with cathode strip chambers (CSC) as the inner layer.

Three layers of resistive plate chambers (RPC) in the barrel ($|\eta| < 1.05$) and three layers of thin gap chambers (TGC) in the end-caps ($1.05 < |\eta| < 2.4$) provide the muon trigger and also measure the muon trajectory in the non-bending plane of the spectrometer magnets.

The ATLAS detector has a three-level trigger system: level 1 (L1), level 2 (L2), and the Event Filter (EF). The MS provides a L1 hardware muon trigger which is based on hit coincidences within different RPC or TGC detector layers inside programmed geometrical windows which define the muon p_{T}. The L2 and EF muon triggers perform a software validation of the L1 muon trigger using additional information from MDT and CSC chambers and from the ID, applying a further p_{T} selection.

3 Classification of reconstructed muons

Three kinds of reconstructed muons are considered in this note:

- **Combined (CB)** muons, obtained from the combination of tracks reconstructed independently in the MS (stand-alone muons) and in the ID;

- **Segment tagged (ST)** muons, obtained from ID tracks that, extrapolated to the MS, are associated with track segments in the muon chambers.

- **Calorimeter tagged (CT)** muons, obtained by matching ID tracks with an energy deposition in the calorimeters compatible with a minimum ionizing particle. These are used in place of ID tracks to reduce the background in the "tag and probe" method.

CB muons are the highest purity muon candidates. ST muons give additional efficiency as they can recover muons which did not cross enough precision chambers to allow an independent momentum measurement in the MS. Typical cases are low p_T muons that only reach the inner layer of precision chambers or less instrumented detector regions.

Two independent reconstruction chains, each implementing CB and ST muons, are used in ATLAS [5]: chain 1 (or Staco) and chain 2 (or MuId). This redundancy allows a cross check of the performances of the reconstruction algorithms and is particularly useful in the the first phase of the LHC operation.

Efficiencies for four categories of reconstructed muons are presented in this note:

- **CB, chain 1:** CB muons from chain 1 with the χ^2 of the MS-ID combination lower than 150 for 5 degrees of freedom. In contrast to other studies [2], no cut on the relative momentum difference between the ID and the MS tracks was applied; the effect of this cut on the efficiency was found to be negligible in the low-p_T region studied in this analysis;

- **CB + ST, chain 1:** all CB muons from chain 1 plus ST muons from chain 1 not associated to a CB muon from the same reconstruction chain;

- **CB, chain 2**: all CB muons from chain 2;

- **CB + ST, chain 2:** all candidates belonging to the previous category plus ST muons not associated to a CB muon from the same reconstruction chain. The algorithm used in this analysis for chain 2 ST muon finding differs from that used in other studies [2] since it is optimised for muon identification at low p_T.

4 Monte Carlo samples and expectations

A Monte Carlo (MC) sample of five million prompt J/ψ events with subsequent decay into muons was generated with PYTHIA 6.4 [6] using the PYTHIA implementation of the colour-octet model. It was then passed through a detailed simulation of the ATLAS detector [7] based on GEANT4 [8, 9] and reconstructed with the same reconstruction programs as real data.

The reconstruction efficiencies obtained from analysis of the Monte Carlo sample are shown in Figure 1 as a function of p_T and η for CB and CB+ST muons from chain 1. The most discernible features are the areas of lower efficiency at fixed η that result from the crack in the MS at $\eta \approx 0$ for the passage of services and from the barrel/end-cap transition region at $|\eta| \approx 1.2$ where the chamber configuration and the magnetic field are rather non-uniform. Another clearly visible feature of Figure 1 is that, for $|\eta| < 2.0$, the CB+ST muons start to be efficient at lower p_T with respect to CB muons since they include muons reaching only the inner layer of muon chambers in the MS. For $|\eta| > 2.0$ the CB and CB+ST efficiency are very similar since cases with only one segment in the CSC chambers, which correspond to the inner layer of precision chambers in this region, are not considered for ST muons. This motivates the binning used in this note for the reconstruction efficiency determination. The data are separated into five pseudorapidity intervals according to the different MS regions:

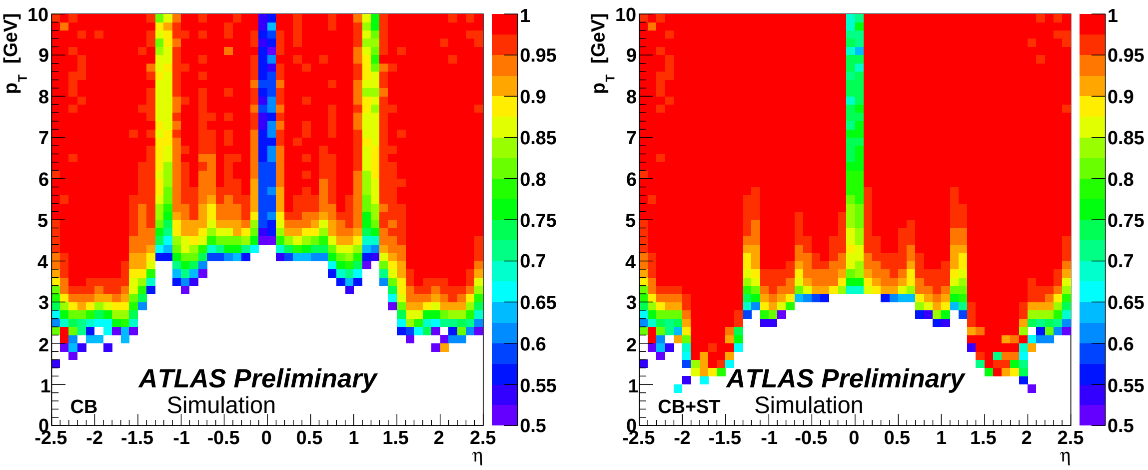

Figure 1: The muon reconstruction efficiency from Monte Carlo for CB (left) and CB+ST (right) muons of the reconstruction chain 1. The efficiency is shown as a function of η and p_{T} for efficiency values above 0.5.

$\lvert\eta\rvert < 0.1$,	the $\eta = 0$ crack region;
$0.1 < \lvert\eta\rvert < 1.1$,	the barrel region;
$1.1 < \lvert\eta\rvert < 1.3$,	the transition region between the barrel and the end-cap;
$1.3 < \lvert\eta\rvert < 2.0$,	the end-cap region;
$2.0 < \lvert\eta\rvert < 2.5$,	the forward region.

5 Selection of Tag and Probe pairs

Events were selected online with a single-muon trigger chain. At level 1 the events were taken by the lowest possible L1 trigger threshold, "L1_MU0". At L2 and at the EF, a CB muon was required, with minimum-p_{T} thresholds of 4, 6 or 10 GeV. As the luminosity increased during the data taking, the two lower p_{T} thresholds were prescaled. Approximatively 35% of the integrated luminosity used in this analysis was collected with the lowest unprescaled threshold of $p_{\mathrm{T}} > 4$ GeV, 50% with $p_{\mathrm{T}} > 6$ GeV and 15% with $p_{\mathrm{T}} > 10$ GeV. For the first part of the considered period, corresponding to $\approx$ 1.5% of the integrated luminosity, the events were selected online using the L1 trigger only.

Good collision events were selected by requiring at least one reconstructed primary vertex with three or more associated good ID tracks, where a good ID track was defined by having:

- ≥ 1 pixel hits;
- ≥ 6 SCT hits;
- for $|\eta| < 1.9$: total number of TRT hits $n^{\mathrm{tot}}_{\mathrm{TRT}} > 5$;
- for $n^{\mathrm{tot}}_{\mathrm{TRT}} > 5$: fraction of outlier TRT hits $n^{\mathrm{out}}_{\mathrm{TRT}}/n^{\mathrm{tot}}_{\mathrm{TRT}} < 90\%$. TRT outliers are measurements associated to the ID track that either appear in a drift tube not crossed by the track or belong to a set of TRT measurements that failed to form a smooth trajectory together with the Pixel and SCT measurements.

A tag muon was defined to have:

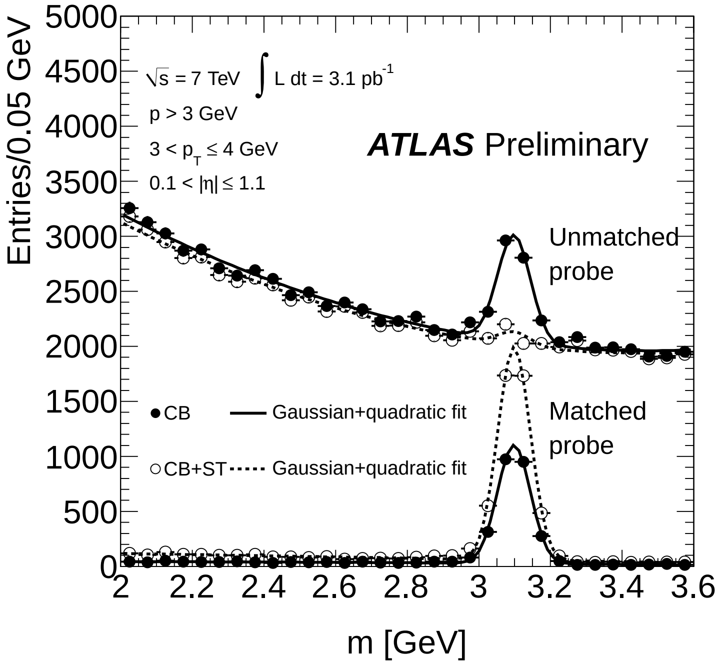

Figure 2: Invariant mass of the unmatched (upper points) and matched (lower points) tag-probe pairs for CB (filled circles) and CB+ST (empty circles) muons of chain 1 for $0.1 < |\eta| < 1.1$ and $3 < p_T < 4$ GeV. The curves show the fits described in the text.

- a CB muon associated to a good ID track defined as above;
- $p_T > 4$ GeV, $|\eta| < 2.5$;
- distance of closest approach to the primary vertex in the transverse plane $|d_0| < 0.3$ mm and in the longitudinal coordinate $|z_0| < 1.5$ mm. Distance of closest approach significances $|d_0|/\sigma(d_0) < 3$ and $|z_0|/\sigma(z_0) < 3$;
- the tag muon is consistent with being the muon that fired the trigger. This was checked by requiring that the reconstructed muon is consistent with passing through the η-ϕ region in the MS (the "region of interest" [4]) corresponding to the trigger muon.

Probes were selected as any good ID track, as defined above, with

- $p > 3$ GeV, $|\eta| < 2.5$;
- the probe and the tag track can be refitted to a common vertex with $\chi^2/\mathrm{ndof} < 6$;
- distance between tag and probe $\Delta R = \sqrt{(\Delta\phi)^2 + (\Delta\eta)^2} < 3.5$.

All possible tag-probe combinations are used in the analysis. The above selection results in 2.6×10^6 tag-probe pairs in the invariant mass range $2.0 < m < 3.6$ GeV, including 276 cases in which the same probe enters in two different pairs.

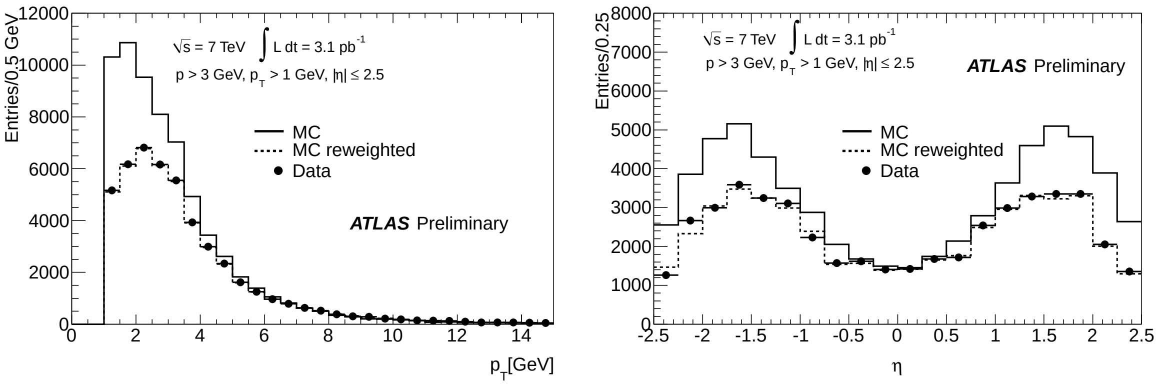

Figure 3: Distribution of probes, after background subtraction, in p_{T} (left) and η (right), for data, MC, and reweighted MC. Tags were selected using chain 1.

6 Efficiency measurement

To measure the reconstruction efficiency of a particular algorithm, the tag-probe pairs were divided into two categories, those in which the probe was reconstructed as a muon by the algorithm (matched) and those in which the probe was not reconstructed as muon (unmatched). Figure 2 shows the invariant mass distribution for pairs with the probe in the transverse momentum and pseudorapidity region $3 < p_{\mathrm{T}} < 4$ GeV and $0.1 < |\eta| < 1.1$. The mass distribution is shown separately for probes classified as matched and unmatched with respect to CB and to CB+ST chain 1 muons. The distribution of matched probes shows a clean peak at the J/ψ mass with low background while the distribution of unmatched probes has a peak on top of a large background.

The reconstruction efficiency was obtained as the the ratio of the number of events in the peak of the matched distribution to the total number of events in the two mass peaks. A χ^2 fit was performed simultaneously on the two distributions, with the following parametrizations:

$$\begin{aligned}
\text{Matched} \quad f_M(m) &= N_{\mathrm{tot}}\,\epsilon\, G(m\,;\,\mu_M,\sigma_M) + P_M(m) \\
\text{Unmatched} \quad f_U(m) &= N_{\mathrm{tot}}\,(1-\epsilon)\, G(m\,;\,\mu_U,\sigma_U) + P_U(m)
\end{aligned}$$

where $G(m;\mu,\sigma)$ is a Gaussian distribution with mean μ and standard deviation σ, used to describe the signal peak, and P is a polynomial function used to describe the background. The main parameters extracted from the fit are the number of tag-probe pairs in the signal peak N_{tot} and the reconstruction efficiency ϵ. The mean and width of the two Gaussian distributions were forced to be the same and second-order polynomials were used for the background.

The MC sample was used to compare the efficiencies obtained with the method described above to the true efficiency, defined as the probability for a true muon matched to a reconstructed ID track to be also reconstructed as a CB or CB+ST muon. The differences were found to be always smaller than 1%. It should be noted that this check does not test the background subtraction procedure since the background is almost absent in the J/ψ MC sample.

Figure 3 shows the number of probes after background subtraction as a function of p_{T} and η for data and MC. The MC distribution differs significantly from the data, being more populated at low p_{T} and large $|\eta|$. This difference is ascribed to several origins: the lack of non-prompt J/ψ production in the MC sample (i.e. J/ψs from beauty decays), possible deficiencies of the physics model, and a distortion caused by the trigger requirements applied on the tag muon in the data but not in the MC.

For a precise comparison of the efficiencies calculated in data and MC it is important that the underlying probe distributions agree. For this reason the MC tag-probe pairs have been reweighted according to the data/MC ratio calculated in small two-dimensional bins in η and p_{T}, using a simple sideband subtraction to extract the J/ψ yield for the data. The probe distributions after reweighting are also shown in Figure 3.

7 Systematic checks and uncertainties

A number of checks have been performed to study the dependence of the results on analysis details and assumptions (the abbreviations in parentheses are used later in Table 1):

1. Signal shapes (s1): the mean and the widths of the two Gaussian functions in the fit were allowed to vary independently.

2. Background shape (s2): a linear background function was used in the fit, instead of the quadratic one, and the fit was performed in a reduced mass range of 2.7 – 3.5 GeV.

3. Alternative fit (s3): a simultaneous fit to the matched and the total (matched + unmatched) distributions, rather than to matched and unmatched, was used to enhance the fit stability.

4. Trigger matching: the bias introduced by the trigger was studied by applying a different criterion, based on a ΔR cut, to associate the tag muon to the trigger muon. The effect was negligible.

5. Other signal extraction methods: to reduce the dependence on the functional form used in the fit, the efficiency was also calculated using sideband subtraction. The analysis was also repeated using the sPlot [10] technique. No significant variation of the efficiency was observed.

6. Dependence on probe selection: the dependence on the probe selection was tested by reducing the background by requiring an energy deposit in the calorimeter compatible with a muon. No significant variation of the efficiency was observed. Further studies with a calorimeter-based probe selection are presented in Section 10.

7. Dependence on the impact parameter cuts: the dependence on the fraction of prompt and non-prompt J/ψ in the sample was checked by loosening the cuts on the track d_0 and z_0 in the selection of the tag muon. No significant variation of the efficiency was observed.

8. Period dependence: the data sample was split in two different periods; the results were compatible within the statistical uncertainties.

The maximal positive and negative variations among checks 1 to 3 were considered as systematic uncertainties and added in quadrature to the statistical uncertainty to obtain the total upper and lower uncertainties.

The efficiency measured in a given bin of p_{T} and η depends on the underlying probe distribution within that bin. Therefore the measured efficiency applies only to a sample of muons with the same p_{T} and η distribution as the probes. In addition to the sources of systematic error described above, the uncertainty from the underlying probe distribution was included when comparing the result with MC (s4). This uncertainty was evaluated by using different procedures to reweight the MC probe distribution. The weights applied to the MC were calculated using alternative methods to extract the J/ψ signal (the same fit used for the efficiency measurement or a simpler sideband subtraction) and using different binnings in p_{T} and η. The variations were in general within 2%.

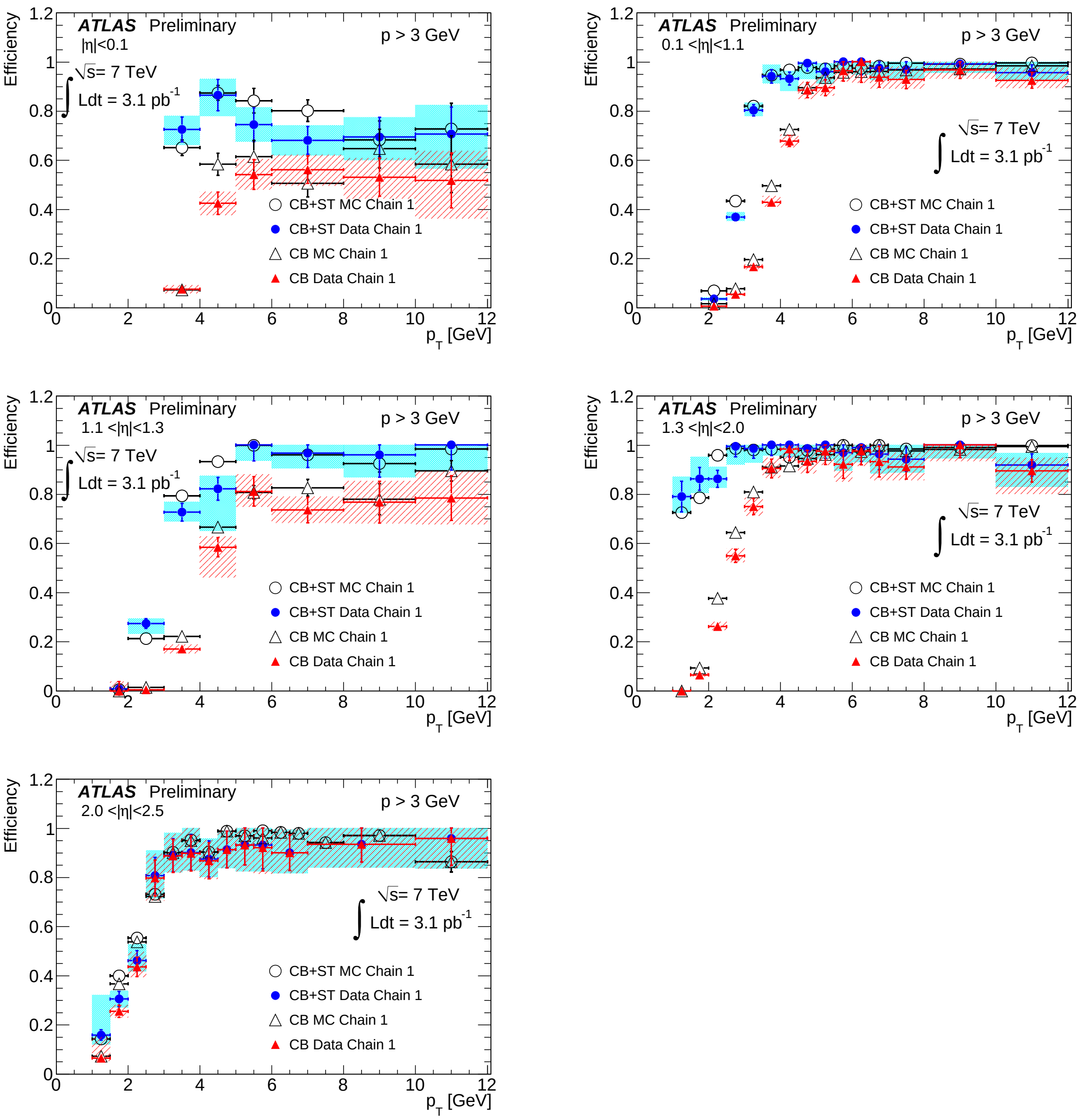

Figure 4: Efficiency for CB and CB+ST muons of chain 1 as a function of p_T for five bins in $|\eta|$ for data and MC. The error bars represent the statistical uncertainties while the band around the data points represents the statistical and systematic uncertainties added in quadrature.

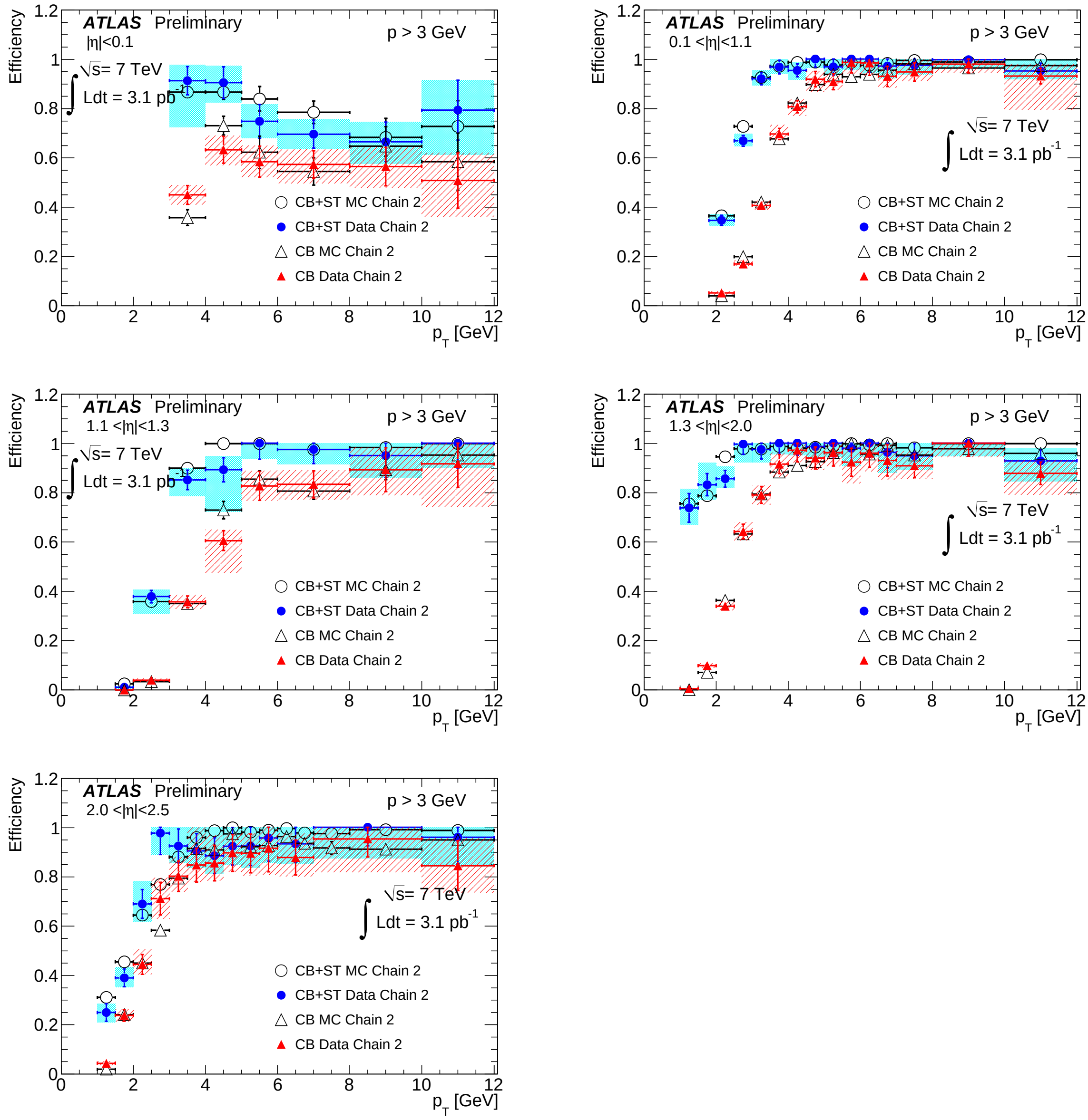

Figure 5: Efficiency for CB and CB+ST muons of chain 2 as a function of p_{T} for five bins in $|\eta|$ for data and MC. The error bars represent the statistical uncertainties while the band around the data points represents the statistical and systematic uncertainties added in quadrature.

8 Reconstruction efficiency with respect to ID tracks

Figure 4 shows the efficiency for chain 1 with respect to ID tracks with $p > 3$ GeV as a function of the probe p_{T} for the five bins in $|\eta|$. As expected, the efficiency for CB+ST muons is larger than for CB muons at low p_{T} and in the η ranges corresponding to the less instrumented regions ($|\eta| < 0.1$ and $1.1 < |\eta| < 1.3$). In the forward region ($2.0 < |\eta| < 2.5$) CB and CB+ST have similar efficiencies. The requirement $p > 3$ GeV only affects the two bins with $p_{\mathrm{T}} < 3$ GeV in the region $0.1 < |\eta| < 1.1$ and the bins with $p_{\mathrm{T}} < 2$ GeV in the region $1.1 < |\eta| < 2.0$. The efficiency plateau is reached for $p_{\mathrm{T}} > 5$ GeV for CB muons and $p_{\mathrm{T}} > 3.5$ GeV for CB+ST muons in the barrel region, while it starts earlier in the end-caps. In the range $|\eta| < 0.1$ the efficiency is larger for p_{T} in the range $4-5$ GeV than at larger p_{T} since low-p_{T} tracks have more chances to be bent away from the $\eta = 0$ crack. In the range $1.3 < |\eta| < 2.0$, the efficiency for CB+ST muons is above 70% for $p_{\mathrm{T}} > 1$ GeV. The simulation describes the data well.

Figure 5 shows the efficiency for chain 2. Also in this case the agreement between data and MC is very good.

The Data/MC scale factors, defined as s.f. $= \epsilon_{\mathrm{data}}/\epsilon_{\mathrm{MC}}$, where ϵ_{data} and ϵ_{MC} are the measured efficiencies for data and MC, are given in Table 1 for the plateau region $p_{\mathrm{T}} > 6$ GeV.

9 Charge dependence

Due to the toroidal magnetic field of the ATLAS MS, muons with positive (negative) charge are bent towards larger (smaller) η. This effect introduces a charge dependence of the muon reconstruction and trigger efficiencies, which is particularly relevant at very large $|\eta|$, where muons of one charge may be bent outside the detector geometrical acceptance, and at low p_{T}, where muons of one charge may be bent back before reaching the middle or outer MS stations.

As an illustration, Figure 6 shows the measured efficiency as a function of η for CB muons of chain 1. The charge dependence of the efficiency is reversed between the two sides of ATLAS: the efficiency for positively charged muons is larger for $\eta < 0$ than for $\eta > 0$, since at $\eta < 0$ (> 0) they are bent away from (towards) the beamline, while the opposite holds for negatively charged muons. Therefore, as long as the ATLAS detector is symmetric with respect to $\eta = 0$, the efficiency depends only on $q \times \eta$, where q is the muon charge. Figures 7 (chain 1) and 8 (chain 2) show the reconstruction efficiency as a function of $q \times \eta$ for two p_{T} regions: $1 < p_{\mathrm{T}} < 6$ GeV and $p_{\mathrm{T}} > 6$ GeV. In the first region a strong asymmetry between positive and negative $q \times \eta$ is observed for CB muons. For CB+ST muons the asymmetry is lower since in this case it is sufficient to find a segment in the inner MS stations, which are located at a position where the muon trajectory has not yet been significantly bent by the toroidal magnetic field. Most of the asymmetry for CB+ST muons is in the largest $|\eta|$ bin. The $q \times \eta$ dependence is well reproduced by the simulation. No significant asymmetry is observed in the high-p_{T} region.

10 Reconstruction efficiency with respect to calorimeter-tagged muons

At large p_{T} the uncertainty of the reconstruction efficiency measurement described above is dominated by the statistical contribution from the background in the unmatched sample. The background can be significantly suppressed using CT muons as probes instead of ID tracks. The CT efficiency for muons from J/ψ decays is around 90%. The same analysis as described above was repeated with the difference that the probe was required to be a CT muon. This allows a precise measurement of the probability that a CT muon is also reconstructed as a CB or CB+ST muon. A cut of $p_{\mathrm{T}} > 4$ GeV was applied by the CT muon algorithm, as the background contamination of CT muons increases rapidly at lower p_{T}. The mass distributions for tag-probe pairs with matched and unmatched probes are shown in Figure 9. As the background is small and linear to a good approximation, a simple sideband subtraction was used to

	$\|\eta\|$ range	s.f.	± stat.	+syst.	-syst.	s1	s2	s3	s4
Chain 1	0.0 : 0.1	1.022	0.084	0.025	-0.042	-0.035	0.004	-0.027	±0.024
CB	0.1 : 1.1	0.973	0.018	0.022	-0.001	0.009	0.016	0.021	±0.001
	1.1 : 1.3	0.909	0.050	0.022	-0.007	0.008	0.021	0.001	±0.007
	1.3 : 2.0	0.951	0.023	0.037	-0.075	-0.075	0.037	-0.025	±0.001
	2.0 : 2.5	0.976	0.056	0.040	-0.013	-0.012	0.040	0.008	±0.003
Chain 1	0.0 : 0.1	0.958	0.155	0.009	-0.019	-0.018	0.004	-0.005	±0.008
CB+ST	0.1 : 1.1	0.989	0.017	0.015	-0.001	$<10^{-3}$	0.015	0.015	±0.001
	1.1 : 1.3	1.024	0.046	0.015	-0.020	-0.015	0.007	0.005	±0.013
	1.3 : 2.0	0.970	0.024	0.036	-0.066	-0.065	0.035	-0.023	±0.006
	2.0 : 2.5	0.976	0.050	0.040	-0.013	-0.012	0.040	0.008	±0.003
Chain 2	0.0 : 0.1	0.930	0.080	0.059	-0.073	-0.042	0.007	-0.034	±0.059
CB	0.1 : 1.1	0.982	0.018	0.024	-0.002	0.008	0.017	0.024	±0.002
	1.1 : 1.3	0.969	0.049	0.021	-0.020	-0.020	0.021	-0.004	±0.001
	1.3 : 2.0	0.962	0.024	0.036	-0.072	-0.072	0.036	-0.022	±0.004
	2.0 : 2.5	0.963	0.053	0.050	-0.029	-0.027	0.050	-0.023	±0.008
Chain 2	0.0 : 0.1	0.922	0.057	0.022	-0.023	-0.009	0.004	$<10^{-3}$	±0.021
CB+ST	0.1 : 1.1	0.992	0.017	0.012	$<10^{-3}$	$<10^{-3}$	0.012	0.012	$<10^{-3}$
	1.1 : 1.3	1.001	0.045	0.007	-0.012	-0.011	0.005	0.003	±0.005
	1.3 : 2.0	0.972	0.023	0.028	-0.063	-0.063	0.028	-0.027	±0.003
	2.0 : 2.5	0.996	0.050	0.015	-0.020	-0.012	0.015	-0.020	±0.003

Table 1: Data/MC scale factors for $p_T > 6$ GeV in different intervals of $|\eta|$. The table shows the scale factor (s.f.), the statistical uncertainty, the total positive and negative systematic uncertainties and the contributions to the systematic uncertainty from individual sources described in the text: signal shape (s1), background shape (s2), alternative fit (s3), and MC reweighting (s4).

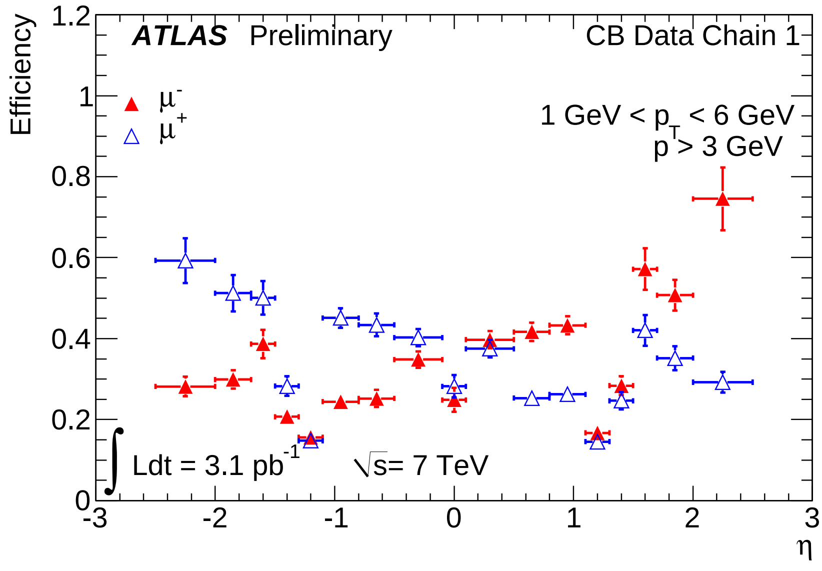

Figure 6: Efficiency for CB muons of chain 1 as a function of η, separately for μ^+ and μ^-. Only statistical uncertainties are shown.

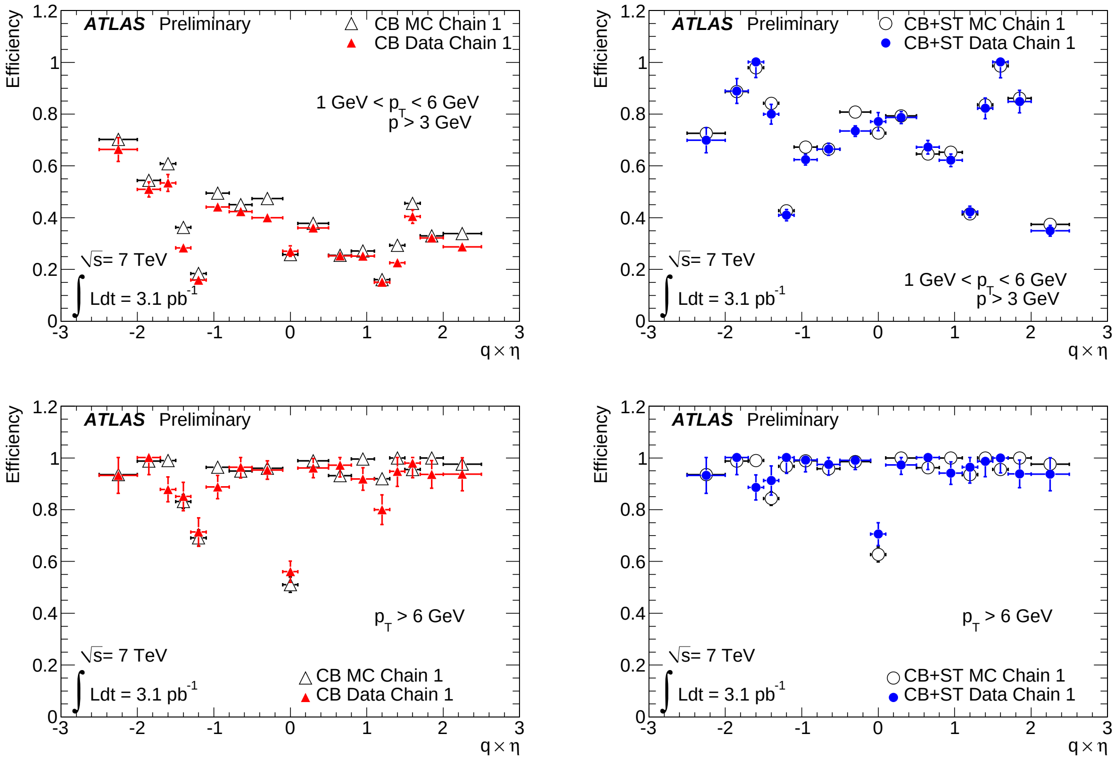

Figure 7: Efficiency for CB (left) and CB+ST (right) muons of chain 1 as a function of $q \times \eta$ for data and MC. The upper plots are for the p_{T} range $1 < p_{\mathrm{T}} < 6$ GeV. The lower plots are for $p_{\mathrm{T}} > 6$ GeV. Only statistical uncertainties are shown.

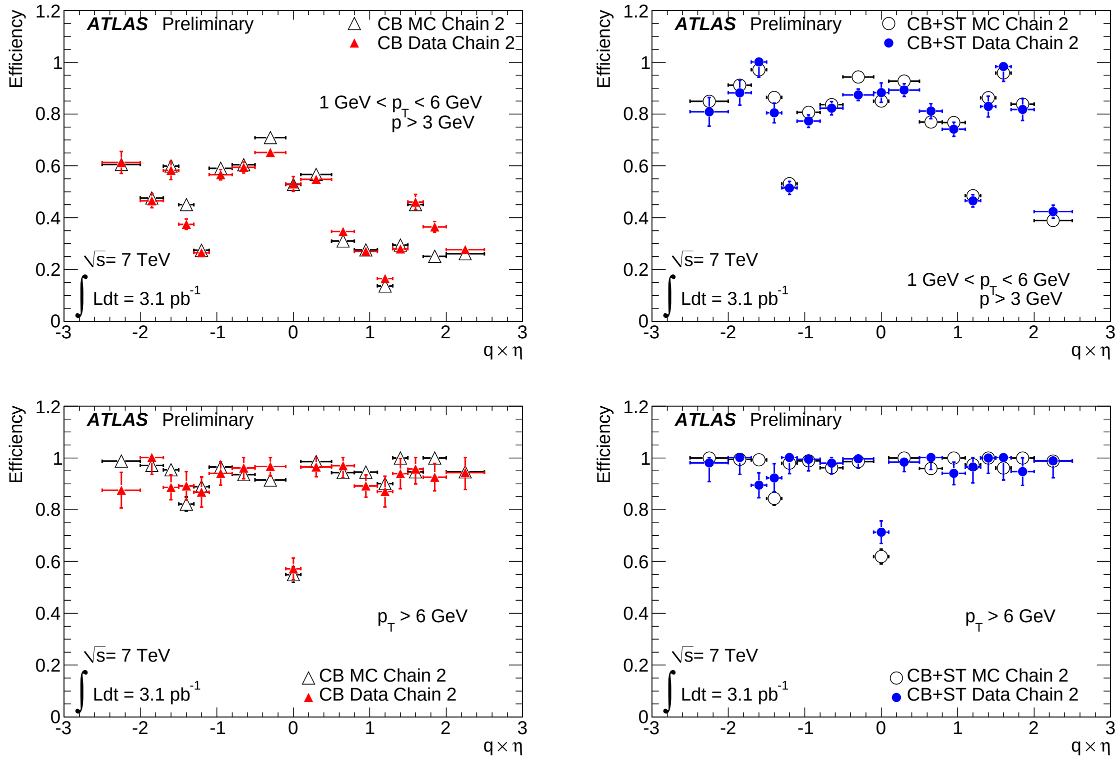

Figure 8: Efficiency for CB (left) and CB+ST (right) muons of chain 2 as a function of $q \times \eta$ for data and MC. The upper plots are for the p_{T} range $1 < p_{\mathrm{T}} < 6$ GeV. The lower plots are for $p_{\mathrm{T}} > 6$ GeV. Only statistical uncertainties are shown.

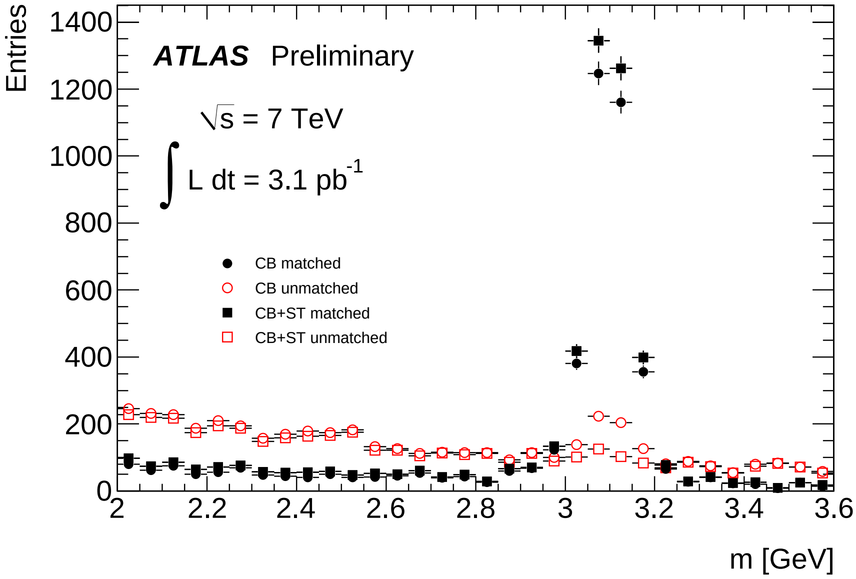

Figure 9: Invariant mass using calorimeter-tagged muons as probes for unmatched and matched tag-probe pairs for CB (filled circles) and CB+ST (empty circles) muons of chain 1 for $0.1 < |\eta| < 1.1$ and $p_T > 4$ GeV.

determine the signal yield using the mass range 2.95 – 3.25 GeV for the signal region, 2.65 – 2.95 GeV and 3.25 – 3.55 GeV for the sidebands. No reweighting of the MC probe distribution was needed since the probe distribution was reasonably described by MC.

The efficiency for CB muons with respect to CT muons is shown in Figures 10 and 11 and compared to the MC results. The following systematic uncertainties were considered:

1. Signal extraction: the signal region was widened to 2.9 – 3.3 GeV and the sidebands moved to 2.5 – 2.9 and 3.3 – 3.7 GeV;

2. Tag muon selection: the trigger matching criteria and the p_T cut on the tag muon were varied, producing negligible effects on the efficiency;

3. MC probe distribution: the η distribution was reweighted by varying by 33% the weight of muons in the end-caps, to allow for differences between data and MC similar to those observed in Figure 3. The effect on the plateau efficiency was ≤ 0.1%.

The effects of the above variations were added in quadrature to the statistical uncertainty to produce the total error bars.

At large p_T the efficiency reaches a plateau of $\approx$ 94% (99%) for CB (CB+ST) muons for both chains. Data and MC agree to within 2%. The data/MC scale factors are given in Table 2 for $p_T > 6$ GeV and the full pseudorapidity range, $|\eta| < 2.5$. These scale factors are in agreement with those for the efficiencies calculated with respect to ID tracks presented in Table 1. The average scale factors obtained in the analysis of high-p_T muons from $Z \to \mu\mu$ decays [2] are also reported in Table 2, showing good agreement between the two analyses.

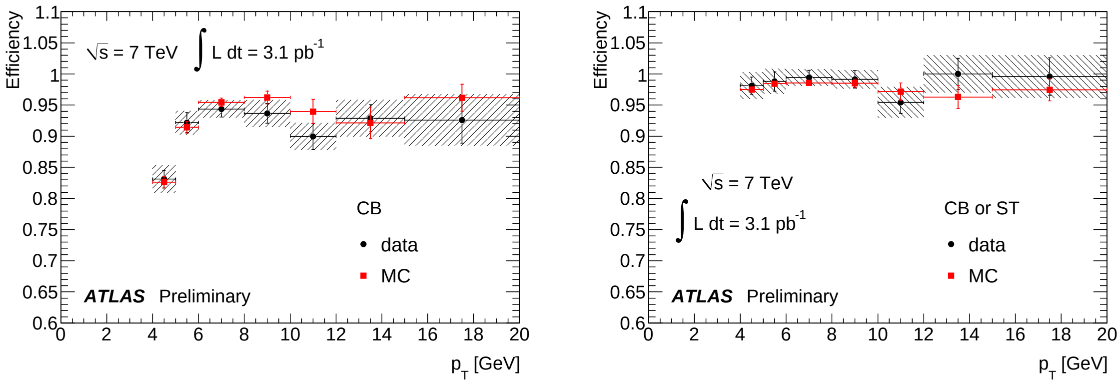

Figure 10: Efficiency of CB (left) and CB+ST (right) muons with respect to calorimeter-tagged muons for chain 1 as a function of p_T for the full range of η. Results for Data and MC are shown. The error bars represent the statistical uncertainties while the band around the data points represents the statistical and systematic uncertainties added in quadrature.

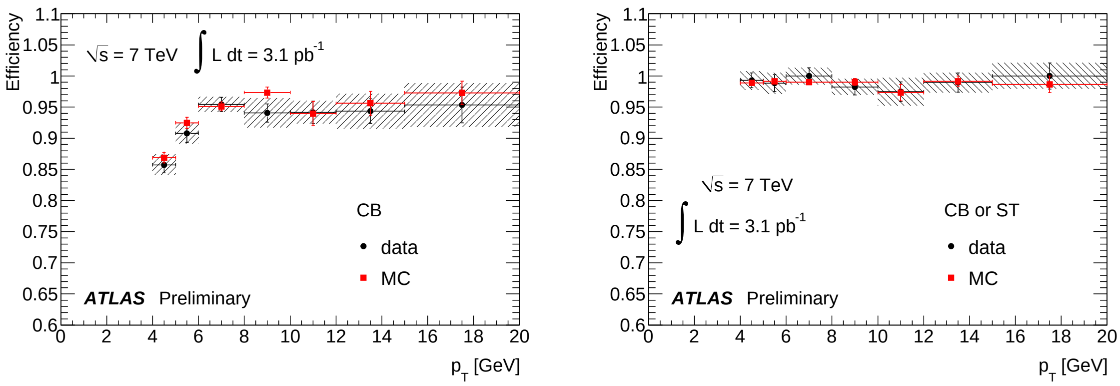

Figure 11: Efficiency of CB (left) and CB+ST (right) muons with respect to calorimeter-tagged muons for chain 2 as a function of p_T for the full range of η. Results for Data and MC are shown. The error bars represent the statistical uncertainties while the band around the data points represents the statistical and systematic uncertainties added in quadrature.

Algorithm		s.f.	± stat.	± syst.	s.f.@Z	± stat.
chain 1	CB	0.980	0.007	0.005	0.9806	0.0024
	CB+ST	1.009	0.004	0.003	0.9990	0.0016
chain 2	CB	0.993	0.007	0.007	0.9918	0.0020
	CB+ST	1.011	0.003	0.005	1.0006	0.0015

Table 2: Scale factors (s.f.) for the efficiency with respect to calorimeter-tagged muons for the full pseudorapidity range $|\eta| < 2.5$ and $p_T > 6$ GeV. The last two columns show the scale factors obtained from the analysis of $Z \to \mu\mu$ decays [2].

11 Trigger efficiency

The "tag and probe" method was also used to measure the trigger efficiency relative to reconstructed muons. The trigger efficiency measurement follows the same approach as the measurement of the reconstruction efficiency, with the main difference being that reconstructed muons are used as a probe. This study also uses the same sample and triggers used in the J/ψ cross section measurement [1]. Two kinds of trigger efficiencies have been measured:

- **$\epsilon(\mathrm{L1}\,|\,\mathrm{rec})$:** the probability for a reconstructed muon to pass the level 1 trigger;
- **$\epsilon(\mathrm{L2}\,\&\,\mathrm{EF}\,|\,\mathrm{L1}\,\&\,\mathrm{rec})$:** the probability for a reconstructed muon accepted by the L1 trigger to pass a particular p_T threshold at level 2 and in the Event Filter.

Figure 12 shows $\epsilon(\mathrm{L1}\,|\,\mathrm{rec})$ for the lowest L1 threshold ("L1_MU0") with respect to chain 1 muons for the regions covered by the RPC ($|\eta| < 1.05$) and the TGC ($1.05 < |\eta| < 2.4$) trigger chambers. The efficiency at plateau ($p_T > 8$ GeV) is $\approx$ 80% (76%) for CB (CB+ST) muons in the barrel and $\approx$ 95% (93%) in the end-cap, in agreement with studies based on inclusive muon samples [11]. The lower efficiency in the barrel region is mainly due to the geometrical acceptance of the trigger systems that have inefficient regions corresponding to support structures of the ATLAS detector. The L1 efficiency for CB muons is higher than for CB+ST muons, in particular at low p_T. This is because the L1 trigger chambers are placed close to the second layer of MDT chambers in the MS. CB muons, that require segments in at least two MDT layers to be reconstructed, are typically made of muons that reach the middle stations, while ST muons, at low p_T, are typically made of muons reaching only the inner MDT stations, therefore missing the trigger chambers.

The efficiency $\epsilon(\mathrm{L2}\,\&\,\mathrm{EF}\,|\,\mathrm{L1}\,\&\,\mathrm{rec})$ is shown in Figure 13 for two p_T thresholds, $p_T > 4$ GeV ("EF_mu4") and $p_T > 6$ GeV ("EF_mu6"). The efficiency above the nominal threshold is 90% or larger.

12 Conclusions

Muons from J/ψ decays have been used to measure the reconstruction and trigger efficiencies of the ATLAS detector for low-p_T muons, using a data set corresponding to an integrated luminosity of $3.1\mathrm{pb}^{-1}$.

The reconstruction efficiency is well described by the Monte Carlo simulation. For $p_T > 6$ GeV the reconstruction efficiency is above 98% and the scale factor, defined as the ratio of data and MC efficiencies ranges from 0.98 to 1.01 depending on the particular type of reconstruction considered.

The efficiency was also measured for the level 1 trigger and for level 2 and event filter triggers used in the J/ψ cross section analysis [1]. The L1 trigger efficiencies, measured using CB reconstructed tracks, reach a plateau value of 80% in the barrel and 95% and endcap region for $p_T > 8$ GeV. The L2 and EF efficiency, above the applied p_T thresholds, is above 90%.

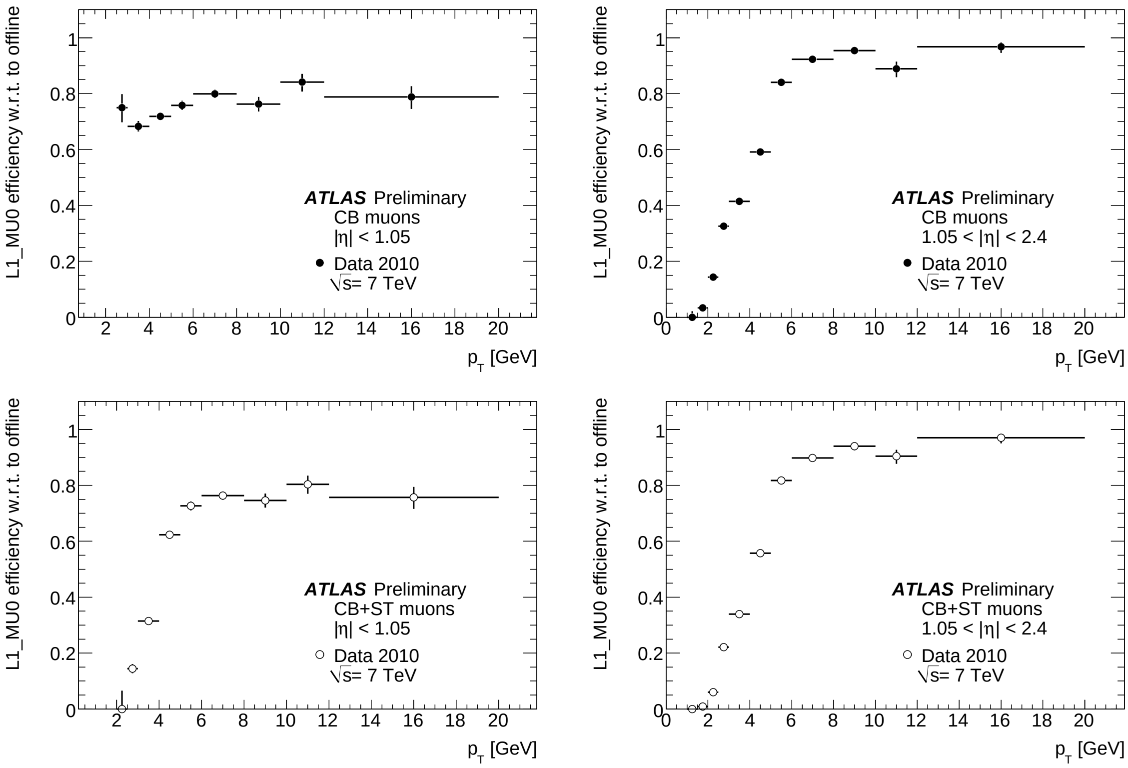

Figure 12: Efficiency $\epsilon(\mathrm{L1}\,|\,\mathrm{rec})$ for the L1 trigger "L1_MU0" with respect to reconstructed chain 1 muons, CB (upper plots) muons as a function of p_{T} for the trigger barrel (left) and end-cap (right) regions. The lower plots show the efficiencies for CB+ST muons.

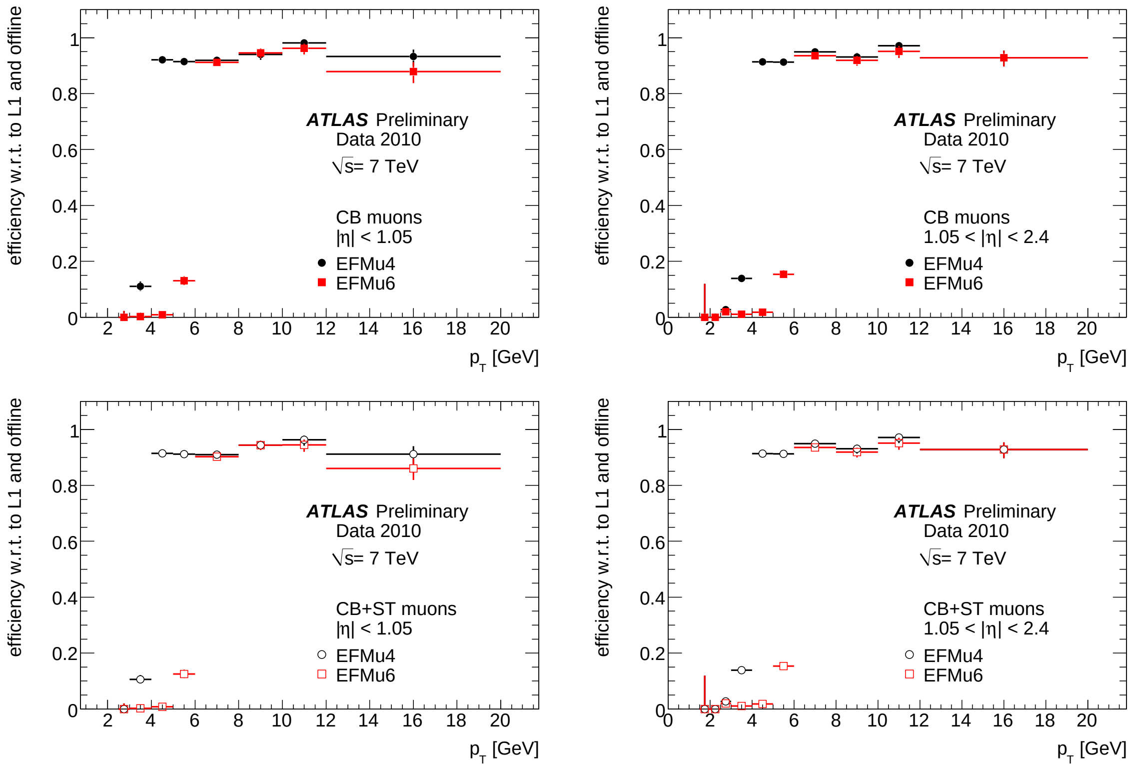

Figure 13: Efficiency $\epsilon(\mathrm{L2}\,\&\,\mathrm{EF}\,|\,\mathrm{L1}\,\&\,\mathrm{rec})$ for the L2 and Event Filter trigger p_{T} thresholds of 4 and 6 GeV with respect to reconstructed chain 1 CB (upper plots) and CB+ST (lower plots) muons that passed the L1 trigger.

References

[1] ATLAS Collaboration, *Measurement of the differential cross sections for the $J/\psi \to \mu^+\mu^-$ resonance and the non-prompt J/ψ cross section fraction with pp collisions at $\sqrt{s} = 7$ TeV*, article in preparation (2011) .

[2] ATLAS Collaboration, *Determination of the muon reconstruction efficiency in ATLAS at the Z resonance in proton-proton collisions at $\sqrt{s} = 7$ TeV*, ATLAS-CONF-2011-008 (2011) .

[3] ATLAS Collaboration, *Muon Reconstruction Performance*, ATLAS-CONF-2010-064 (2010) .

[4] ATLAS Collaboration, G. Aad et al., *The Atlas Experiment at the CERN Large Hadron Collider*, JINST **3** (2008) S08003.

[5] ATLAS Collaboration, *Muon Performance in Minimum Bias pp Collision Data at $\sqrt{s} = 7$ TeV with ATLAS*, ATLAS-CONF-2010-036 (2010) .

[6] T. Sjostrand, S. Mrenna, and P. Z. Skands, *PYTHIA 6.4 Physics and Manual*, JHEP **05** (2006) 026.

[7] ATLAS Collaboration, G. Aad et al., *The ATLAS Simulation Infrastructure*, Eur. Phys. J. **C70** (2010) 823–874, arXiv:1005.4568.

[8] S. Agostinelli et al., *Geant4 a simulation toolkit*, Nuclear Instrument and Methods A **506** (2006) no. 3, 250 –303.

[9] J. Allison et al., *Geant4 developments and applications*, Nuclear Science, IEEE Transactions on **53** (2006) no. 1, 270 –278.

[10] M. Pivk and F. Le Diberder, *sPlot: a statistical tool to unfold data distributions*, arXiv:0402083v3.

[11] ATLAS Collaboration, *Performance of the ATLAS Muon Trigger in p-p collisions at $\sqrt{s} = 7$ TeV*, ATLAS-CONF-2010-095 (2010) .